Research Article | Vol. 27, No. 5 | 4 Mar 2019 | OPTICS EXPRESS 6792
Optics EXPRESS

Fabrication of a nanofiber Bragg cavity with high quality factor using a focused helium ion beam

HIDEAKI TAKASHIMA,[1,3] ATSUSHI FUKUDA,[1,3] HIRONAGA MARUYA,[1] TOSHIYUKI TASHIMA,[1] ANDREAS W. SCHELL,[1,2] AND SHIGEKI TAKEUCHI[1,*]

[1]*Department of Electronic Science and Engineering, Kyoto University, Kyoto daigaku-katsura, Nishikyo-ku, Kyoto 615-8510, Japan*
[2]*Central European Institute of Technology, Brno University of Technology, 612 00 Brno, Czech Republic*
[3]*These authors contributed equally to this work*
takeuchi@kuee.kyoto-u.ac.jp

Abstract: Nanofiber Bragg cavities (NFBCs) are solid-state microcavities fabricated in an optical tapered fiber. NFBCs are promising candidates as a platform for photonic quantum information devices due to their small mode volume, ultra-high coupling efficiencies, and ultra-wide tunability. However, the quality (Q) factor has been limited to be approximately 250, which may be due to limitations in the fabrication process. Here we report high Q NFBCs fabricated using a focused helium ion beam. When an NFBC with grooves of 640 periods is fabricated, the Q factor is over 4170, which is more than 16 times larger than that previously fabricated using a focused gallium ion beam.

1. Introduction

Efficient coupling of photons emitted from single light emitters into a single-mode fiber is attractive for photonic and quantum applications, such as bio-sensors [1], low-threshold lasers [2], and photonic quantum information devices [3–6]. In this context, optical nanofibers are an excellent platform for such applications. Optical nanofibers are tapered optical fibers with a radius less than the visible wavelengths at the tapered region [7, 8]. They have a high transmittance of almost unity and low-loss interconnection to single-mode fibers. They also have a large evanescent field in the thin region known as the taper waist. For these properties, nanofibers can realize the efficient input/output of photons to the single mode fiber via the taper waist without a microscope objective. Nanofibers have thus been used as waveguides to couple photons into solid-state microcavities [9, 10]. Furthermore, they can efficiently couple photons emitted from single light emitters into the fundamental mode of a single-mode fiber [11, 12]. We have developed an efficient single photon source with a coupling efficiency of more than 7% by locating CdSe/ZnS quantum dots on the nanofiber [13]. In addition to this demonstration, there have been many coupling experiments between nanofibers and single light emitters such as quantum dots [14, 15], molecules [16], nitrogen vacancy centers in diamond [17–20], and hexagonal boron nitride [21].

Nanofiber cavities, which are optical microcavities embedded in nanofibers, have been developed to further improve the coupling efficiency [22–26]. We have recently developed nanofiber Bragg cavities (NFBCs) using a gallium-ion type focused ion beam (FIB). These NFBCs have a single resonant mode with small mode volume (in the order of λ^3) [25]. Coupling of a CdSe/ZnS quantum dot with the NFBC was demonstrated, and the Purcell enhancement and coupling efficiency when a single light emitter was placed on the surface of the NFBC was also numerically analyzed [27]. However, the quality (Q) factors of the NFBCs were approximately 250. A cavity structure of air-nanohole arrays was very recently fabricated on a nanofiber [26, 28]. However, the Q factors of the previously reported NFBCs have been limited to a value of several

#354585 https://doi.org/10.1364/OE.27.006792
Journal © 2019 Received 4 Dec 2018; revised 18 Jan 2019; accepted 29 Jan 2019; published 22 Feb 2019

Optics EXPRESS

hundred [25, 26].

We now aim to improve two aspects of the NFBCs to achieve better Q factors; to reduce contamination and achieve better resolution. The first issue is contamination by Ga ions during the fabrication process, which may cause optical losses. The second issue is the accuracy of the resolution of the Ga FIB. In our previous work, we used a Ga FIB (SMI2050) with a resolution of a few tens of nanometers, which was insufficient to fabricate the small nanostructures. All previous fabrications of NFBCs employed Ga FIB.

In this letter, we report high Q factor NFBCs fabricated using a focused helium ion beam (He FIB) [29]. When an NFBC with grooves of 640 periods was fabricated, the best Q factor that was achieved (limited by the spectrometer) was 4170, which is over 16 times larger than that previously reported using a Ga FIB.

2. Methods

2.1. Fabrication of NFBC using focused helium ion beam

An optical nanofiber was first fabricated by heating a single-mode optical fiber (Thorlab 630HP) with a ceramic heater and stretching it into a fine thread [8, 30]. The waist diameter was reduced to approximately 300 nm, which maintained single-mode propagation. The nanofiber was fixed on a U-shaped metal holder using UV adhesive [Fig. 1(a)]. Pigtails at both ends of the nanofiber are rolled and fixed on the holder using Kapton tape.

Figure 1(b) shows the He FIB (ZEISS "Orion NanoFab") [29]. A tungsten tip with a three-sided pyramid, referred to as a trimer, is used as a source to produce the ion beam. A high voltage is applied to the tip, which produces an extremely high electric field at the apex of the tip. When He atoms are flowed over the tip, they are attracted to the apex of the tip and ionized. He ions are then emitted from one atom of the trimer and focused onto the sample after passing through an aperture, lenses, and scanning deflectors. A resolution of less than 1 nm can be achieved with the He FIB, due to the short de Broglie wavelength of helium, which is much smaller than the corresponding electron wavelength. Unlike the Ga FIB, the He FIB is contamination-free because the gaseous ions go out from the matrix of the sample after fabrication.

The He FIB is periodically irradiated from the top side of the nanofiber. The beam current, the ion dose, and the dwell time are typically ca. 1 pA, 1.6×10^{-3} C/cm^2, and 1 μs, respectively. By scanning the focused ion beam perpendicularly to the direction of the long axis of the nanofiber, the silica glass was sputtered and periodic grooves were fabricated on the nanofiber. For irradiation from the top side, the groove of the grating is an arch-like shape, as shown in Fig. 2(a). A defect to function as a cavity is introduced between the two gratings. Three types of NFBCs with total grating periods of 160, 320, and 640 were fabricated to adjust the Q factor. The fields of view for each grating period for fabrication were 60 μm, 120 μm, and 240 μm, respectively.

Figure 2(b) shows a scanning ion microscope (SIM) image of the NFBC with a grating period of 160. The diameter of the nanofiber was estimated to be 310 nm. A defect is observed between the two Bragg gratings with periodical grooves. The depth of the groove, the length of the pitch, and the length of the defect were 30 nm, 320 nm, and 840 nm, respectively.

2.2. Optical property measurement of the NFBCs

Transmission spectra were measured to evaluate the optical properties of the NFBCs. A halogen lamp (AQ4305, Yokogawa) connected with a single-mode fiber was used as the light source. The polarization of the light from the single-mode fiber was fixed as linear using a polarizer. After the polarizer, the polarization of the light is adjusted using a polarization controller, which consists of a half-wave plate and a quarter-wave plate, so that the difference between the peak value of the resonant peak and the bottom of the stop band becomes a maximum. The light

Optics EXPRESS

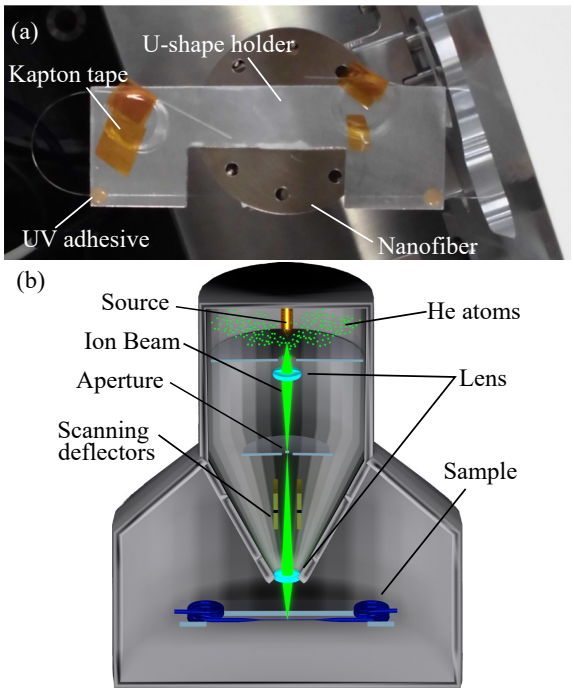

Fig. 1. (a) Photograph of the NFBC fixed on a U-shaped metal holder. (b) Schematic illustration of the He FIB.

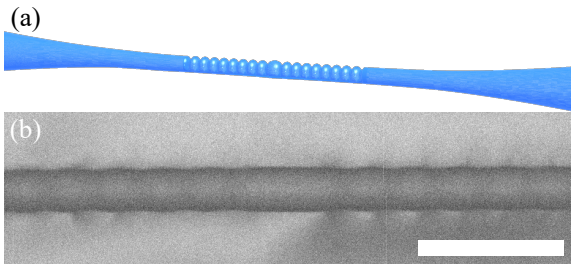

Fig. 2. (a) Schematic illustration of the NFBC. (b) SIM image of the NFBC. The scale bar is 1 μm.

passing through the polarization controller is connected to the input port of the NFBC. The light from the output port of the NFBC is measured using a spectrometer (MS257, Oriel Instruments) with a grating of 1800 grooves and a CCD camera (DU420-OE, Andor). The spectral resolution of the spectrometer was 0.17 nm. The transmission spectra were normalized with respect to the transmission of a non-tapered single-mode fiber.

2.3. FDTD simulation for the optical property of the NFBCs

The numerical simulations given in the latter part of this letter are based on a three-dimensional (3D) finite-difference time-domain (FDTD) simulation using a commercial package (FDTD Solutions, Lumerical) [27]. The calculation area for the FDTD simulation was set to $106 \times 2 \times 2$ μm^3. The diameter of the nanofiber, the depth of the groove, and the length of the defect used in the calculation model were set to 310 nm, 30 nm, and 840 nm, respectively. These

Optics EXPRESS

parameters were estimated from the SIM image [Fig. 2(b)]. The detailed method to simulate the transmittance spectra of the NFBCs is given elsewhere [27].

3. Results and discussion

3.1. Transmission spectrum for the NFBC fabricated using He FIB

Figure 3(a) shows the measured transmission spectrum for the NFBC with a grating period of 160 fabricated using the He FIB shown in Fig. 2(b). The transmittance of the nanofiber was approximately 0.5, which is different from the numerical simulation [Fig. 3(b)] for ideal condition. This is due to the losses for the imperfection of the nanofiber structure, the dust on the surface of the nanofiber, and damage to the nanofiber during the fabrication process. A sharp resonant peak appeared inside the stop band of the Bragg grating with a width of approximately 8 nm. The height of the peak is almost same as the transmittance outside the stop band. The resonant wavelength and the linewidth of the peak are 673.8 nm and 1.5 nm, respectively, which correspond to a Q factor of 450. The difference of the resonant peak from the center of the stop band is due to the cavity length being 840 nm, which is different from the $\lambda/4$-shifted defect.

Figure 3(b) shows the calculated transmission spectrum. The shape of the calculated spectrum is almost in agreement with the experimental result shown in Fig. 3(a). The length of the groove pitch is set to 320 nm, which was estimated from the SIM image [Fig. 2(b)]. The calculated Q factor is 490. The difference of the resonant peak from the center of the stop band is also reproduced in the calculated spectrum. The inset of Fig. 3(b) shows the calculated cross section of the normalized electric field distribution at the resonant wavelength. The electric field becomes a maximum at the center of the cavity. Outside the fiber, large evanescent fields appeared because the diameter of the fiber (310 nm) is less than half of the resonant wavelength.

Next, these results were compared with the previously observed transmittance spectra of a NFBC fabricated using the Ga FIB [Fig. 3(c)] [25]. The total number of the grating periods is 160. The observed Q factor was improved from approximately 250 for the NFBC fabricated using the Ga FIB. In addition, the transmission of the spectrum and the shape of the resonant peak were also improved due to the improved resolution of the He FIB and a reduction in contamination during the fabrication process.

3.2. Effect of the grating periods on the transmission spectrum

To improve the Q factor, the total number of grating periods was increased to 320. Figure 4(a) shows the measured transmission spectrum for the NFBC with 320 grooves. The diameter of the nanofiber was 304 nm. A sharper resonant peak than that for the NFBC with a grating period of 160 appeared inside the stop band. The wavelength of the peak was 701.78 nm. The linewidth of the peak was 0.4 nm, which is compensated by deconvolution of the linewidth of the spectrometer. From the wavelength and the linewidth, the Q factor was estimated to be 1750. The height of the peak became slightly smaller than the transmittance outside the stop band, which is due to scattering of the light coupled to the NFBC to outside the nanofiber with an increase in the Q factor by the grating loss [27].

Figure 4(b) shows the calculated transmission spectrum. The length of the groove pitch was set to 335 nm. The resonant wavelength and the linewidth of the peak were 701.37 nm and 0.25 nm, respectively. These results are in agreement with a Q factor of 2800. The height of the resonant peak became smaller than the transmittance outside the stop band as observed in the experimental transmission spectrum. The linewidth of the stop band was also somewhat broader than the experimental result. This difference is considered to be due to the inhomogeneity of the structure caused by charging up of the nanofiber during the fabrication process, the reduction of the resolution by the large field of view, and the increase in defects induced by the irradiation in the glass matrix [33].

Optics EXPRESS

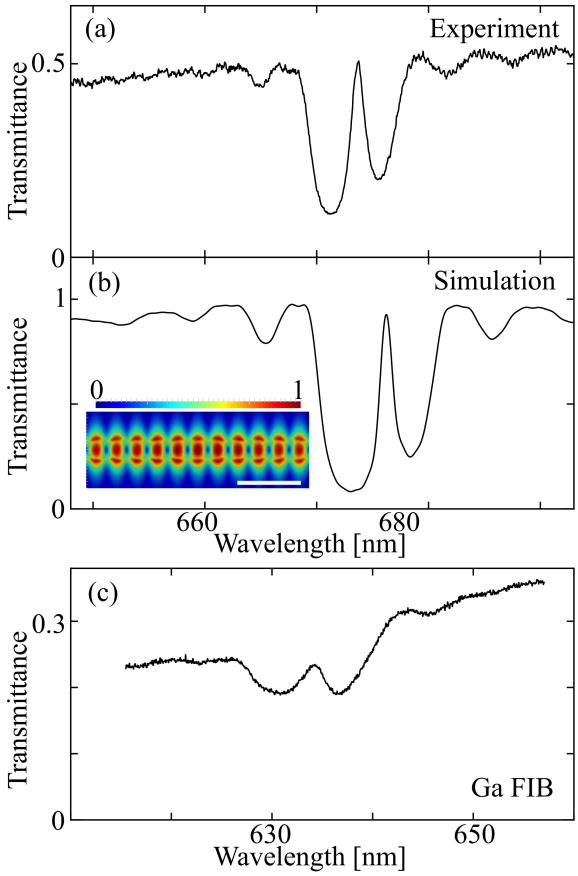

Fig. 3. (a) Normalized transmission spectrum for the NFBC fabricated using the He FIB. The numbers of the grooves is 160. (b) Calculated transmission spectrum. The inset shows the electric field distribution at the resonant wavelength using the 3D FDTD simulation. The scale bar is 1 μm. (c) Normalized transmission spectrum for the NFBC fabricated using the Ga FIB.

To further improve the Q factor, the total number of grating periods was increased up to 640. Figure 5 shows the observed transmission spectrum for this NFBC. However, the numerical simulation of the structure using the FDTD was beyond the available computational power. The diameter of the nanofiber was 306 nm. A resonant peak appeared at 699.80 nm inside the stop band. The linewidth of the resonant peak was 0.17 nm. These results correspond to a Q factor of 4170. The spectral resolution limited by the grating and the spectrometer was 0.17 nm; therefore, the actual linewidth of the resonant peak was narrower than this value and means that the actual Q factor is larger than 4170, which is at least 16 times larger than the NFBC fabricated using the Ga FIB.

Optics EXPRESS

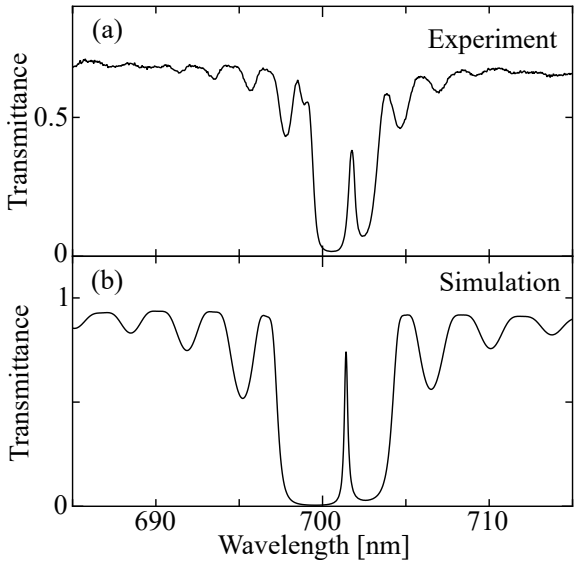

Fig. 4. (a) Measured transmission spectrum and (b) calculated transmission spectrum for an NFBC with 320 grooves.

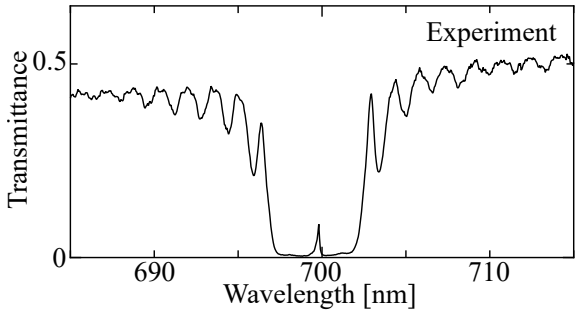

Fig. 5. Normalized transmission spectrum for an NFBC with 640 grooves.

3.3. *Numerical estimation of the coupling efficiency achievable using the realized NFBCs*

When the single light emitter is placed at a maximum of the electric field in the cavity, the enhancement factor P of the photon emission is given by the Purcell formula: [9, 31]

$$P = \frac{3}{4\pi^2}\left(\frac{\lambda}{n}\right)^3 \frac{Q}{V_{\text{eff}}}, \tag{1}$$

where n is the refractive index. V_{eff} is the effective mode volume. It is defined as [27, 31, 32]

$$V_{\text{eff}} = \frac{\int_V \epsilon(\mathbf{r})|\mathbf{E}(\mathbf{r})|^2 d^3\mathbf{r}}{\max[\epsilon(\mathbf{r})|\mathbf{E}(\mathbf{r})|^2]}, \tag{2}$$

where $\epsilon(\mathbf{r})$ is the dielectric constant and $\mathbf{E}(\mathbf{r})$ is the electric field. The NFBC with a total grating period of 160 had a Q factor of 450 and an effective mode volume of 2.3 μm^3. Taking these

Optics EXPRESS

values into account, P was estimated to be 1.5. When the total grating number was increased to 320 and 640, P was estimated to be at least 6.5 and 15.3, respectively.

When there is no propagation loss at the grating of the NFBC, the coupling efficiency η is expressed as a ratio of the cavity-modified emission rate into the nanofiber to the total emission rate as follows [34],

$$\eta = \frac{P\gamma_f}{\gamma_0 + P\gamma_f}, \tag{3}$$

where γ_0 is the rate of spontaneous emission into radiation modes and γ_f is the rate of the spontaneous emission into the nanofiber.

Here we assume that the coupling efficiency of the nanofiber without the cavity structure is 0.3, *i.e.*, the rate of γ_f and γ_0 is 3/7. Under this assumption, the coupling efficiency η of the NFBC with P = 1.5 becomes 0.39. η for the NFBCs with P = 6.5 and 15.3 also increase to 0.74 and 0.87, respectively. Note that the reduction of the transmission would cause the decrease in the coupling efficiency of the actual device.

4. Conclusion

In conclusion, we have reported the fabrication of high-quality (Q) factor nanofiber Bragg cavities fabricated using a helium FIB. When the NFBC was fabricated with 160 grooves, the observed Q factor increased to 450 from Q = 250 for our previous NFBC fabricated using a Ga FIB. As the number of the grooves was increased up to 640, the Q factor of the NFBC was over 4170, which was the resolution limit of the spectrometer. These improvements were due to the improved resolution and reduced contamination with the He FIB.

The transmission of the resonant peak decreased when the number of the grooves was increased. To prevent this reduction, it would be useful to fabricate low-loss structures, such as sinusoidal or tapering grooves [35–37]. We consider that the development of high Q NFBCs will be beneficial for the realization of fiber-integrated quantum information devices that exploit a large Purcell enhancement [3–6].

Funding

Japan Society for the Promotion of Science (JSPS) (Nos. 21101007, 26220712, 23244079, 25620001, 23740228, 26706007, 26610077, and 16K04918); Core Research for Evolutional Science and Technology (CREST) (JPMJCR1674); Matsuo Foundation; International Research Fellow of the JSPS.

Acknowledgments

The authors would like to thank Dr. Kimihiro Norizawa at the Institute of Scientific and Industrial Research of Osaka University for the support for FIB fabrication. We gratefully acknowledge financial support in the form of Kakenhi Grants-in-Aid (Nos. 21101007, 26220712, 23244079, 25620001, 23740228, 26706007, 26610077, and 16K04918) from the Japan Society for the Promotion of Science (JSPS) and from the CREST program of the Japan Science and Technology Agency (JST) (JPMJCR1674). H. T. acknowledges the support of the Matsuo Foundation. A.W.S. acknowledges support as an International Research Fellow of the JSPS. A portion of this work was supported by the "Nanotechnology Platform Project (Nanotechnology Open Facilities in Osaka University)" of the Ministry of Education, Culture, Sports, Science and Technology (MEXT), Japan [F-16-OS-0015, F-17-OS-0029, F-18-OS-0019, F-18-OS-0020].

Optics EXPRESS

References

1. F. Vollmer, L. Yang, and S. Fainman, "Label-free detection with high-Q microcavities: A review of biosensing mechanisms for integrated devices," Nanophotonics **1**, 267–291 (2012).
2. H. Yokoyama, "Physics and device applications of optical microcavities," Science **256**, 66–70 (1992).
3. M. Pelton, C. Santori, J. Vučković, B. Zhang, G. S. Solomon, J. Plant, and Y. Yamamoto, "Efficient Source of Single Photons: A Single Quantum Dot in a Micropost Microcavity," Phys. Rev. Lett. **89**, 233602 (2002).
4. S. Takeuchi, "Recent progress in single-photon and entangled-photon generation and applications," Jpn. J. Appl. Phys. **53**, 030101 (2014).
5. H. Oka, H. F. Hofmann, S. Takeuchi, and K. Sasaki, "Effects of Decoherence on the Nonlinear Optical Phase Shift Obtained from a One-Dimensional Atom," Jpn. J. Appl. Phys. **43**, 7495–7500 (2004).
6. H. P. Specht, C. Nölleke, A. Reiserer, M. Uphoff, E. Figueroa, S. Ritter, and G. Rempe, "A single-atom quantum memory," Nature **473**, 190–193 (2011).
7. L. Tong, F. Zi, X. Guo, and J. Lou, "Optical microfibers and nanofibers: A tutorial," Opt. Commun. **285**, 4641–4647 (2012).
8. M. Fujiwara, K. Toubaru, and S. Takeuchi, "Optical transmittance degradation in tapered fibers," Opt. Express **19**, 8596–8601 (2011).
9. K. J. Vahala, "Optical microcavities," Nature **424**, 839–846 (2003).
10. H. Takashima, K. Kitajima, Y. Tanaka, H. Fujiwara, and K. Sasaki, "Efficient optical coupling into a single plasmonic nanostructure using a fiber-coupled microspherical cavity," Phys. Rev. A **89**, 021801 (2014).
11. F. Le Kien, S. D. Gupta, V. I. Balykin, and K. Hakuta, "Spontaneous emission of a cesium atom near a nanofiber: Efficient coupling of light to guided modes," Phys. Rev. A **72**, 032509 (2005).
12. M. Almokhtar, M. Fujiwara, H. Takashima, and S. Takeuchi, "Numerical simulations of nanodiamond nitrogen-vacancy centers coupled with tapered optical fibers as hybrid quantum nanophotonic devices," Opt. Express **22**, 20045–20059 (2014).
13. M. Fujiwara, K. Toubaru, T. Noda, H.-Q. Zhao, and S. Takeuchi, "Highly Efficient Coupling of Photons from Nanoemitters into Single-Mode Optical Fibers," Nano Lett. **11**, 4362–4365 (2011).
14. R. Yalla, F. Le Kien, M. Morinaga, and K. Hakuta, "Efficient channeling of fluorescence photons from single quantum dots into guided modes of optical nanofiber," Phys. Rev. Lett. **109**, 063602 (2012).
15. K. M. Shafi, W. Luo, R. Yalla, K. Iida, E. Tsutsumi, A. Miyanaga, and K. Hakuta, "Hybrid System of an Optical Nanofibre and a Single Quantum Dot Operated at Cryogenic Temperatures," Sci. Rep. **8**, 13494 (2018).
16. A. Stiebeiner, O. Rehband, R. Garcia-Fernandez, and A. Rauschenbeutel, "Ultra-sensitive fluorescence spectroscopy of isolated surface-adsorbed molecules using an optical nanofiber," Opt. Express **17**, 21704–21711 (2009).
17. T. Schröder, M. Fujiwara, T. Noda, H.-Q. Zhao, O. Benson, and S. Takeuchi, "A nanodiamond-tapered fiber system with high single-mode coupling efficiency," Opt. Express **20**, 10490–10497 (2012).
18. L. Liebermeister, F. Petersen, A. V. Münchow, D. Burchardt, J. Hermelbracht, T. Tashima, A. W. Schell, O. Benson, Meinhardt, A. Krueger, A. Stiebeiner, A. Rauschenbeutel, H. Weinfurter, and M. Weber, "Tapered fiber coupling of single photons emitted by a deterministically positioned single nitrogen vacancy center," Appl. Phys. Lett. **104**, 031101 (2014).
19. X. Liu, J. Cui, F. Sun, X. Song, F. Feng, J. Wang, W. Zhu, L. Lou, and G. Wang, "Fiber-integrated diamond-based magnetometer," Appl. Phys. Lett. **103**, 143105 (2013).
20. I. V. Fedotov, L. V. Doronina-Amitonova, D. A. Sidorov-Biryukov, N. A. Safronov, A. O. Levchenko, S. A. Zibrov, Blakley, H. Perez, A. V. Akimov, A. B. Fedotov, P. Hemmer, K. Sakoda, V. L. Velichansky, M. O. Scully, and A. M. Zheltikov, "Fiber-optic magnetometry with randomly oriented spins," Opt. Lett. 39, 6755–6758 (2014).
21. A. W. Schell, H. Takashima, T. T. Tran, I. Aharonovich, and S. Takeuchi, "Coupling Quantum Emitters in 2D Materials with Tapered Fibers," ACS Photonics **4**, 761–767 (2017).
22. K. P. Nayak, P. Zhang, and K. Hakuta, "Optical nanofiber-based photonic crystal cavity," Opt. Lett. **39**, 232–235 (2014).
23. J. Keloth, K. P. Nayak, and K. Hakuta, "Fabrication of a centimeter-long cavity on a nanofiber for cavity quantum electrodynamics," Opt. Lett. **42**, 1003–1006 (2017).
24. K. P. Nayak, F. Le Kien, Y. Kawai, K. Hakuta, K. Nakajima, H. T. Miyazaki, and Y. Sugimoto, "Cavity formation on an optical nanofiber using focused ion beam milling technique," Opt. Express **19**, 14040-14050 (2011).
25. A. W. Schell, H. Takashima, S. Kamioka, Y. Oe, M. Fujiwara, O. Benson, and S. Takeuchi, "Highly Efficient Coupling of Nanolight Emitters to a Ultra-Wide Tunable Nanofibre Cavity," Sci. Rep. **5**, 9619 (2015).
26. W. Li, J. Du, V. G. Truong, and S. N. Chormaic, "Optical nanofiber-based cavity induced by periodic air-nanohole arrays," Appl. Phys. Lett. **110**, 253102 (2017).
27. H. Takashima, M. Fujiwara, A. W. Schell, and S. Takeuchi, "Detailed numerical analysis of photon emission from a single light emitter coupled with a nanofiber Bragg cavity," Opt. Express **24**, 15050–15058 (2016).
28. W. Li, J. Du, and S. N. Chormaic, "Tailoring a nanofiber for enhanced photon emission and coupling efficiency from single quantum emitters," Opt. Lett. **43**, 1674–1677 (2018).
29. B. W. Ward, J. A. Notte, and N. P. Economou, "Helium ion microscope: A new tool for nanoscale microscopy and metrology," J. Vac. Sci. Technol. B **24**, 2871–2874 (2006).
30. H. Konishi, H. Fujiwara, S. Takeuchi, and K. Sasaki, "Polarization-discriminated spectra of a fiber-microsphere system," Appl. Phys. Lett. **89**, 121107 (2006).

Optics EXPRESS

31. L. Andreani and G. Panzarini, "Strong-coupling regime for quantum boxes in pillar microcavities: Theory," Phys. Rev. B **60**, 13276–13279 (1999).
32. K. Srinivasan, M. Borselli, O. Painter, A. Stintz, and S. Krishna, "Cavity Q, mode volume, and lasing threshold in small diameter AlGaAs microdisks with embedded quantum dots," Opt. Express **14**, 1094–1105 (2006).
33. Y.-C. Wang, L. Tian, F. Liu, Y.-B. Qin, G. Zheng, J.-T. Wang, E. Ma, and Z.-W. Shan, "Helium Ion Microscope Fabrication Causing Changes in the Structure and Mechanical Behavior of Silicon Micropillars," Small **13**, 1601753 (2017).
34. F. Le Kien and K. Hakuta, "Cavity-enhanced channeling of emission from an atom into a nanofiber," Phys. Rev. A **80**, 053826 (2009).
35. M. Palamaru and P. Lalanne, "Photonic crystal waveguides: Out-of-plane losses and adiabatic modal conversion," Appl. Phys. Lett. **78**, 1466–1468 (2001).
36. C. Sauvan, G. Lecamp, P. Lalanne, and J. P. Hugonin, "Modal-reflectivity enhancement by geometry tuning in Photonic Crystal microcavities," Opt. Express **13**, 245–255 (2005).
37. M. W. McCutcheon and M. Loncar, "Design of a silicon nitride photonic crystal nanocavity with a Quality factor of one million for coupling to a diamond nanocrystal," Opt. Express **16**, 19136–19145 (2008).